Geological Quarterly, 2021, 65: 23
DOI: http://dx.doi.org/10.7306/gq.1591

Modifications of methods for the fracture analysis from borehole data in application to shale formations

Kinga BOBEK[1, *] and Marek JAROSIŃSKI[1]

[1] Polish Geological Institute – National Research Institute, Rakowiecka 4, 00-975 Warszawa, Poland

Bobek, K., Jarosiński., M., 2021. Modifications of methods for the fracture analysis from borehole data in application to shale formations. Geological Quarterly, 65: 23, doi: 10.7306/gq.1591

Associate Editor: Paweł Aleksandrowski

Systematic joints play an important role in effective fluid conductivity and in the mechanical response of shale reservoirs to hydraulic fracturing. Specific features of joints, such as their strata-bound aspect, and their attitude, commonly normal to bedding, make it necessary to modify standard methods of their analysis from borehole data. Our study, based on borehole core and microresistivity image logs, is adjusted to typical exploration procedure, with vertical boreholes penetrating subhorizontal beds. This simple configuration makes it possible to measure the true height of most joints. We have used joint height as the weighting parameter for the construction of orientation diagrams and for computation of fracture intensity profiles. We also propose here a method for evaluation of fracture orientation error on directly oriented core, show how to distinguish joints present in the scanner record but absent from the core, and how to apply this kind of data filtering to core/log correlation. We also propose to extend the analysis of mineralized joints by using the type and degree of vein cracking in order to better characterize their susceptibility to hydraulic stimulation. Application of the modified methods revealed a stratification of joint distribution which, in some cases, may not be observed due to the scarcity of joint data from boreholes.

Key words: fracture intensity, joints, shale complex, well logging, boreholes.

INTRODUCTION

The geometry and statistical parameters of fracture networks in hydrocarbon reservoirs have long been investigated in order to determine both their impact on effective rock mass permeability (Narr, 1991; Odling, 1997; Odling et al., 1999; Nelson, 2001; Guerriero et al., 2013, 2015; Grasselli et al., 2015; Lorenz and Cooper, 2020) and the response of reservoirs to hydraulic fracturing treatment (Gale et al., 2007, 2014; Salehi and Ciezobka, 2013; Taghichian et al., 2014). Natural fractures, especially penetrative ones with a high degree of connectivity, create additional space for hydrocarbon accumulation and reduce the volume of non-productive zones (Engelder et al., 2009). On the other hand, some large-scale faults and open fractures may lead to a leakage of hydrocarbons out of a reservoir or cause problems with water flood recovery (Wiprut and Zoback, 2000; Li, 2014). Among other types of fractures, joints are especially important for shale reservoirs due to their abundance, penetrative character and regional regularity in their orientation (Helgeson and Aydin, 1991).

In spite of the frequent occurrence of joints in shale, most of them are neglected in Discrete Fracture Network models of shale reservoirs due to their predominantly small size (Li and Lee, 2008; Fu et al., 2013; Bobek et al., 2017). However, even moderate fractures, ~1 m long, are able to nucleate micro-seismic events during hydraulic stimulation (Johri and Zoback, 2013) and, thus, may participate in effective permeability stimulation. There are also other features of joints, e.g. the large range in their size, their strata-bound character and orientation normal to bedding (Fig. 1; Gale et al., 2007; Engelder et al., 2009; Hooker et al., 2013) that make them, in our opinion, not yet properly included in shale reservoir characterization. The present-day software used by the petroleum industry is adjusted to the interpretation and statistical processing of large and medium-sized fractures intersecting with a borehole. In such a general case, the true height of the fractures is unknown and not included in statistical analysis. A contrasting situation occurs when small-scale joints are addressed, these comprising most fractures observed in shale, including our study. As the axis of a vertical borehole is subparallel to steep joint planes, a large number of observed joints reveal their true height. The term true height is used by us in opposition to apparent height, which applies when only a part of the fracture height is observed. One of the aims of this study is to incorporate the true height parameter into statistical analysis of fractures using borehole data.

The most complete characterization of a natural fracture network is possible from surface exposure studies. In such

* Corresponding author, e-mail: kbob@pgi.gov.pl

Received: September 10, 2020; accepted: March 26, 2021; first published online: June 1, 2021

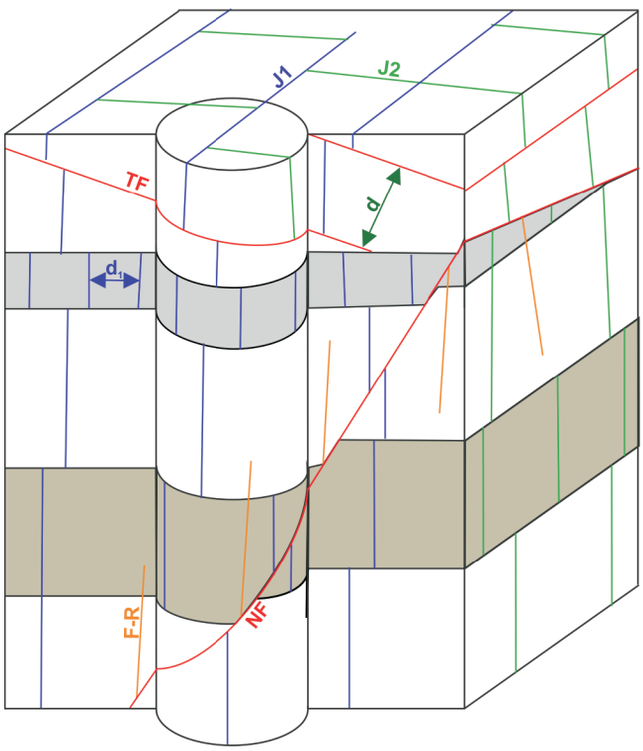

Fig. 1. Scheme of fractures in a horizontally layered shale succession and their representation in a vertical borehole

Subvertical joints of two regional sets J1 and J2 (in blue and green) have geometry unfavourable for being recorded in a vertical borehole, though the true height of such joints may be commonly documented. Due to the separation between joints (d1), which is often greater than the borehole diameter, the distance between joints is rarely observed in borehole data. Gently dipping thrust faults (TF) and steeply dipping normal faults (NF) are preferentially oriented to be penetrated by a vertical borehole. Their distance (d) is often possible to assess, but not their true height. Fractures related to normal faults, fault-related (F-R) are in orange

cases, several statistical methods are used: the linear scanline method; areal sampling; rectangular window sampling; and the circular scanline method (for an overview see Watkins et al., 2015). In a simple tectonic setting, where the fracture network geometry is dominated by a consistent joint system of regional extent (e.g., Engelder et al., 2009), studies of exposures enable the collection of a wide range of attributes of the fracture system, such as spacing, length, orientation of fracture sets, intersection, and others (Boro et al., 2014). However, most of these attributes are not accessible solely from borehole data. By contrast with exposure-based studies, the reliable reconstruction of a fracture network from borehole logs or cores is a challenge. This is mostly because of the small volume of available rock or of borehole wall surface. Borehole imaging tools commonly cover a borehole wall that encloses a cylindrical space ~20 cm in diameter (Brown et al., 2015), which is also the case in our study. The diameter of the borehole core is roughly twice as small. For these values, one may estimate that in a 50 m-thick shale reservoir, the total volume of core from one vertical borehole is <0.5 m^3, while the volume of such a borehole interval is close to 2 m^3. This raises doubts about the possibility of obtaining a reliable fracture distribution from this small rock sample (Peacock, 2006), especially in the case of unfavourable geometry of a sub-vertical borehole and joints. This significant limitation of structural borehole data encouraged us to look at joints in more detail than is usual in the petroleum industry.

An important parameter in the characterization of fracture systems or individual joint sets is their intensity. Several authors have proposed solutions for fracture intensity estimation from borehole data (Dershowitz et al., 2000; Barthélémy et al., 2009; Massiot et al., 2017). Other authors (Lerche and Narr, 1986; Narr, 1991) assumed that the average or median spacing between parallel fractures is linearly related to bed thickness (Ladeira and Price, 1981; Wu and Pollard, 1995) and developed a probabilistic method of quantifying the real joint density. This approach cannot be widely used because the postulated ratio between bed thickness and fracture spacing does not hold in many cases (Mandal et al., 1994; Laubach et al., 2018), as in the shale successions discussed in this paper (Bobek and Jarosiński, 2018). Several other factors control fracture spacing, such as the mechanical stratigraphy or pore pressure compartmentalization in shale successions (Van Noten and Sintubin, 2010). The average fracture spacing method proposed by Narr (1996) is free of the assumption relating fractures to bed thickness. The borehole is treated as a 3D sample and an average fracture spacing (S_{av}) is simply expressed as a ratio of core/borehole diameter (C_d) and height (C_h) product, to the sum of fracture heights (F_h) in the core [1]:

$$S_{av} \quad \frac{C_d \quad C_h}{\sum_{i=1}^{n} F_h} \qquad [1]$$

The results obtained can be easily converted to a fracture intensity parameter and used for reservoir characterization, with the assumption that the fractures collected are representative of the whole population. Our approach is a modification of the above method, tailored to the study of the strata-bound joints.

Each fracture orientation measurement has a limited accuracy, associated with both the unevenness of the measured surface and the deviation of reference direction from the north. In case of a directly oriented core, in addition to the systematic errors of measurements (Nelson et al., 1987), there is an error that one may try to estimate. This error is dependent on the possible core displacement in the core box along the borehole axis and the rate of the tool rotation. In our approach, we estimate the variability of such an error, and then show how this uncertainty can be included in the diagram of joint strike orientation.

In this article we present simple modifications of standard methods of joint analysis adapted to the configuration of vertical exploration wells and jointed horizontal shale successions. The modifications concern the scope of observation features, statistical analyses of joints, and their portrayal in diagrams and data filtering in order to compare the borehole core and joint log records. Our paper does not provide results of a systematic regional fracture study, but instead borehole data are used in it to show the representativeness of the features analysed and to test the modified methods. In order to emphasize the practical context of joint analysis, some comments and references to the hydraulic stimulation treatment of a shale reservoir are included also in the methodological sections. In this contribution, we consequently use the term “joints” for systematic fractures grouped in orientation sets regardless of their extensional, tensional, or shear origin, which is not a common industrial practice (Gale et al., 2014). The term “fracture” is used in an inclusive sense when not only joints are meant but also e.g. fault-related fractures. We use the term “joints” also for veins which have the similar geometry as joints due to similar methods of their statistical analysis. According to our observations, they have the same origin as joints, but were mineralized in further evolution of the shale basin. Similarly, fault-related fractures and veins are also included, if they are subvertical, and planar as are joints. These

rare features are combined with joints, in what we regard as acceptable simplification in our study addressing statistical analysis methods.

DATASET AND GEOLOGICAL CONTEXT

The dataset for application of our methods comes from six exploration boreholes located in the Pomerania region (northern Poland; Fig. 2A, B), from which we obtained in total 1005.3 m of borehole core (of which 449.64 m is directly oriented to the north) and profiles of microresistivity images (X-tended Range Micro Imager – XRMI) 1439.5 m long. The depth correlation between the XRMI and core was performed by our industrial partner. The results obtained contain values of the core/log shift for every core box, which vary between 0 to 3.5 m, with the most common shift equal to ~1 m. However, the results of our study called into question the accuracy of this correction (see chapter 3.4). The boreholes are typically deviated from vertical by <3°, exceptionally reaching up to 6.9° deviation. Intervals covered by the data comprise an Ordovician to lower Silurian rock succession, consisting of shale, claystone, and siltstone with carbonate concretions or interbeds. These shale successions accumulated in a distal part of the Caledonian foredeep basin (Fig. 2A; Poprawa et al., 1999) located on the margin of the East European Craton, where the strata lie at almost horizontally and lack symptoms of any significant tectonic deformation. Sections exposed in boreholes are not affected by major faults; only minor sub-seismic faults or slickensides are present. The lithostratigraphic sequence, of little variation between boreholes, is divided into four main shale formations that, from top to bottom, are the Pasłęk, Jantar (black shale), Prabuty, and Sasino (black shale) formations (Fig. 2C; Feldman-Olszewska and Roszkowska-Remin, 2016; Podhalańska et al., 2016).

For the purpose of this study, we have made macroscopic structural observations of the borehole core with the help of a hand lens. For simplicity and being limited by the resolution of the geophysical data, we assumed the minimum height of the analysed joints to be 2 cm in the core profile and 5 cm on the XRMI log image. A general picture of the joint pattern in the Baltic Basin (Fig. 2) reveals two orientation sets that create a regional system, with more local joint sets occurring in the vicinity of faults or flexures (Bobek and Jarosiński, 2018). The primary regional set of joints (J1), represented in each borehole analysed, striking NNE–SSW, is generally most frequent. However, in the boreholes located in the vicinity of seismic-scale faults, this primary joint set may become subordinate. The secondary regional joint set (J2), striking WNW–ESE, creates almost an orthogonal joint system with the J1 set (Fig. 2B). In the boreholes located far from faults, the secondary set of joints is poorly represented.

JOINTS IN THE BOREHOLE DATA

THE PRESENCE OF JOINTS AND THEIR ATTRIBUTES

During structural profiling of the core, we described such tectonic structures as joints, mineral veins, cracked veins, other bare fractures and slickensides (Doblas, 1998; Fig. 3). The dataset analysed in this study is limited to barren and mineralized joints of dips equal to or exceeding 50° which, in total, account for >95% of the observed tectonic fractures (excluding bedding fractures). In particular boreholes, the contribution of the gently dipping tectonic fractures varies between 0% and 26.8% in core data and never exceeds 6.2% in the XRMI dataset (Table 1). The remaining fractures, steep, planar, without striation, were considered to represent joints. These joints are common in the boreholes studied (Table 1), with their number ranging from 41 in the 130 m long borehole core interval up to 365 in the 310 m long interval. The XRMI profiles have recorded even more joints due to the diameter of the scanned borehole being twice as large as that of the core. In the case of the XRMI data, the number of joints varies in a range from 45 in the 160 m long interval up to 735 in the 301 m long profile. Drilling-induced tensile fractures (Schmitt et al., 2012; Lorenz and Cooper, 2017) were very rarely observed in the scanner image of the borehole wall as well as in the shape of centerline fractures in the borehole core. Joints enhanced by drill mud pressure were observed more often in the scanner record (Bobek and Jarosiński, 2018). In most cases, we consider misinterpretation of joints and drilling-induced tensile fractures unlikely due to the common mineralization of joints and the NNW–SSE direction of the present-day horizontal tectonic stress, oblique to both main joint set directions.

A description of joints visible in borehole core comprises the attributes important for statistical analysis: the dip angle and dip direction azimuth, depth of the upper termination, height, a note on the character of joint termination in vertical and kinematic aperture with mineralization type (fibrous or blocky crystals). Additionally, the type and degree of secondary vein cracking was evaluated. In rare cases, where more than one joint was observed, the separation, type of contact and angle of intersection between joints were recorded. The height has always been measured parallel to the borehole axis which, due to the negligible deviation, is assumed vertical. All joint attributes are stored in the database with hyperlinks to their photographic documentation.

In the case of large fractures oblique to borehole axes, their terminations in the vertical direction go beyond the borehole space, so that their true height is not observable. However, in vertical boreholes, steeply-dipping strata-bound joints terminate very often within the borehole/core space. In the boreholes studied, the true height of joints was determined for almost 90% of joints visible in the borehole core. On average, only 9.3% of joints in core examined exceed the observation space in vertical dimension from one side and 1.6% from both sides. In the scanner data, joints with the known true height comprise almost 80% of all observed fractures, while 19.0% extend beyond the observation space from one side and 1.2% from both sides. The true height of joints rarely exceeds 0.5 m, which is comparable to bed thickness. However, due to the borehole diameter limitation, the general rule is that the larger the joint is, the lower the chance to observe its true height. The highest joint measured in the core is 2 m, while in the scanner image, it reaches 4.3 m due to the larger dimensions of a borehole than those of a core. Determination of the joints' true height creates a new opportunity for more precise structural reservoir characterization.

CRACKED VEINS IN BOREHOLE CORE

Cement-containing joints creating veins are very common in the boreholes studied (Gale et al., 2007, 2014). Most veins are completely mineralized (bearing no vugs) with calcite, but the veins developed on joints are commonly secondarily cracked (Fig. 4A). Such features as the type of secondary cracking and percentage of the vein surface that is secondarily cracked are often neglected in structural core analysis. This is probably because such vein cracking is considered a result of technological core relaxation. In our opinion, no matter how the cracks developed, they might provide useful information about

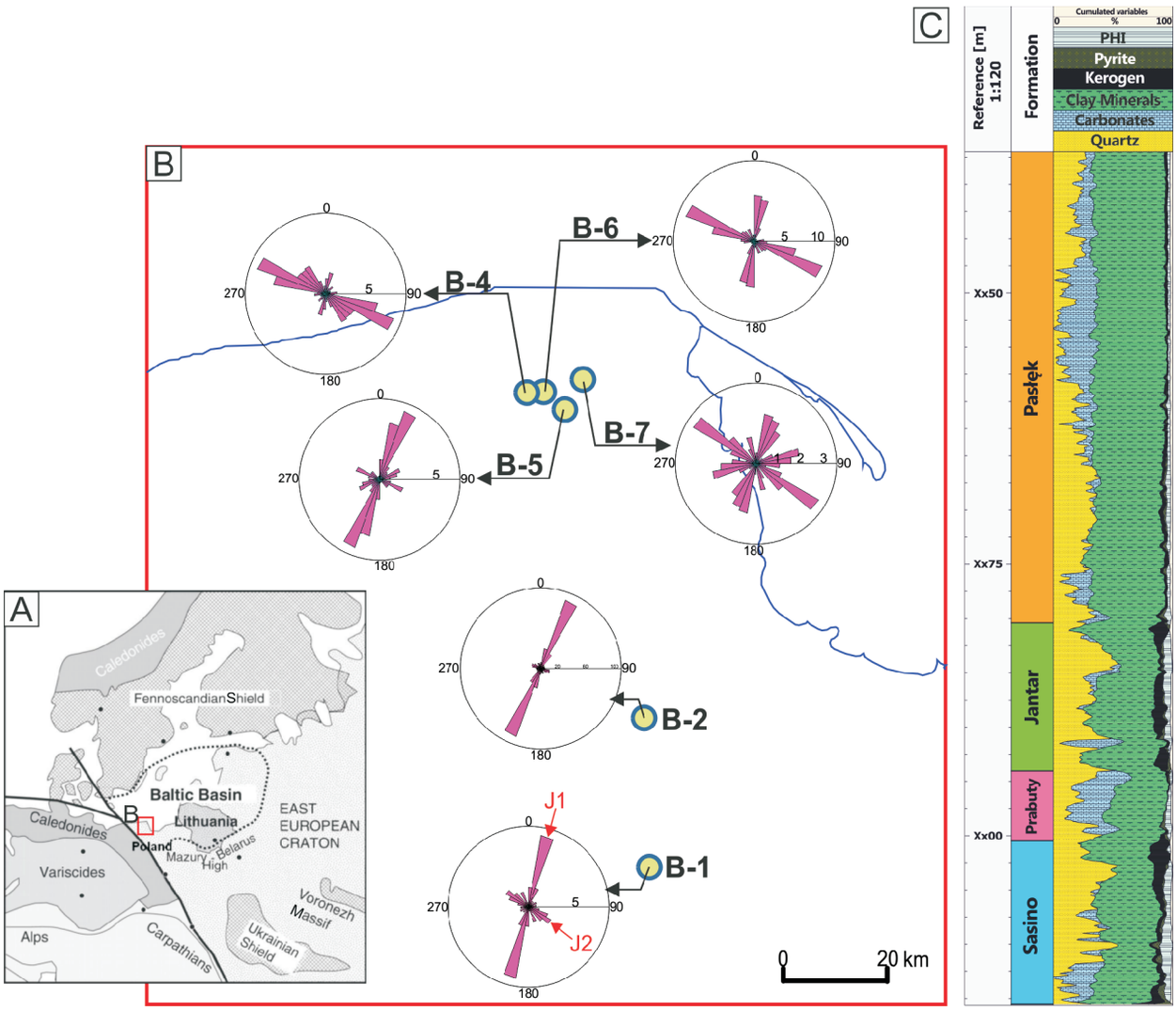

Fig. 2. Location of reference boreholes within a tectonic sketch of Central Europe

A – the range of the Baltic Basin is marked by the dotted line; **B** – location of the boreholes investigated with rose diagrams of the joints' strike obtained from XRMI image interpretation, the two prominent joint sets J1 and J2 are marked by red arrows in the rose diagram from borehole B-1; **C** – typical lithostratigraphic profile of the shale successions analysed based on ULTRA log analysis from the B-2 borehole

the mechanical response of a vein to relaxation. Core unloading and relaxation is, to some extent, a process similar to the effective stress drop during hydraulic stimulation treatment, when the effective minimum stress in the reservoir drops below zero (Zoback et al., 2012). However, the analogy is not perfect because an effective relaxation due to hydraulic stimulation takes place in a tectonically loaded reservoir, and thus tectonic stresses also control the orientation of stimulated fractures. In the case of a borehole core, the tectonic stress beneath the bottom of the borehole is disturbed by the adjacent borehole filled with mud fluid and by the additional load of the core bit. Then, the tectonic stresses are gradually replaced by technological loads induced by drilling, until a complete relaxation during core extraction to the surface when the decreasing mud fluid pressure is the only external force acting on the core surface. Subsequently, most of the relaxation occurs in external isotropic stress conditions that enhance the mechanical weakness of veins despite their orientation. Taking into account the complexity of fracture unloading and relaxation, and that the process differs from hydraulic fracturing, the results of the proposed observations should be interpreted with caution, as they can provide only one piece of information concerning the tendency of veins to crack.

The number of cracked veins in the core and the way in which veins split is dependent on the cohesion of the planes of weakness, which is controlled, among other factors, by the style of mineralization. The planes of weakness might run within the vein or along the interface with the host rock. The style of vein splitting influences the hydraulic communication between the open fracture and shale matrix. The massive calcite seal stuck to the fracture wall can reduce gas seepage towards the stimulated fracture from one or both sides. Such detail may significantly affect gas extraction, especially when veins are common and prone to reactivation in the present-day stress field (Zoback et al., 2012b; Johri and Zoback, 2013). Our two regional joint sets, which are almost entirely mineralized, are oriented diagonally to the present-day maximum stress (Jarosiński, 2006) and therefore should be prone to reactivation in the current strike-slip stress regime. Hence, we can predict that these veins would crack due to hydraulic stimulation and create conductive

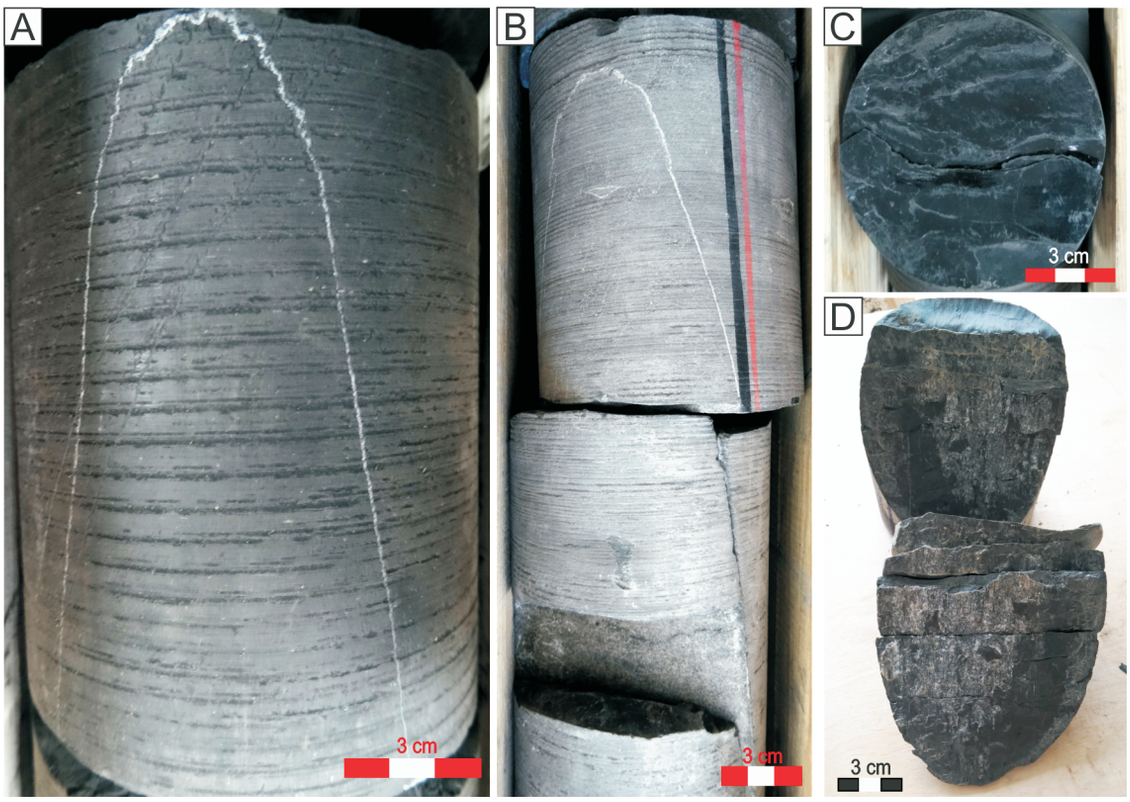

Fig. 3. Tectonic structures observed in core samples from the boreholes

A – sealed vein; **B** – partially cracked vein; **C** – thrust fault slickensides; **D** – normal fault slickensides

fracture network. For this reason, the analyses presented above may be of much importance for estimation of the efficiency in receiving gas from the shale matrix, a process which would be significantly reduced by mineralization.

Syntaxial and antitaxial types of veins (Ramsay and Huber, 1987) with the tendency to crack either within the mineral infill (central suture) or along the vein/rock interface, have been studied. Visual evaluation of the percentage of cracked surfaces was made, to check whether the veins are prone to cracking due to effective relaxation. Then, this parameter is averaged for a joint system (for the unoriented core) or for distinguished joint sets (for the oriented core), taking into account the size of each vein, expressed by its height. This observation gives a semi-quantitative indication of vein cohesion or tensional strength. If the veins are intensely or entirely cracked in the relaxed core, the cohesion might be assumed negligible. By contrast, if the veins are not cracked, cohesion should be considered in the mechanical model of the reservoir.

In the boreholes investigated, the majority of veins are at least partially open (Table 2). The lowest percentage of cracked vein surfaces (36.4% in average for a borehole) was found in the B-5 borehole. The highest values (86.8%) were obtained for the B-7 borehole. These cracks typically split veins leaving parts of the mineral seal on both sides of the crack (Fig. 4A). Mineral infill remaining on both sides of cracked veins seems to be unfavourable for gas exploitation. This factor can be taken into account in the interpretation of hydraulic fracturing effectiveness, but to do so, the appropriate observations have to be made during structural core profiling.

Detailed reservoir characteristics should attribute parameters listed in Table 2 to individual lithological/mechanical units. For instance, in contrast to other formations, in the Prabuty Fm.

Table 1

Comparison of the total fracture number with the number of joints interpreted in the core and XRMI images of the study boreholes

Borehole	Core data				XRMI data			
	Length of core profile [m]	Number of all fractures	Number of joints	% of joints	Length of logged interval [m]	Number of all fractures	Number of joints	% of joints
B-1	130.2	56	41	73.2	159.6	45	45	100.0
B-2	309.7	388	365	94.1	300.7	740	735	99.3
B-4	120.4	159	152	95.5	143.3	284	276	97.2
B-5	123.6	145	133	91.7	188.4	81	76	93.8
B-6	128.9	201	191	95.1	535.5	105	99	94.3
B-7	192.5	115	102	88.7	112.0	98	96	98.0

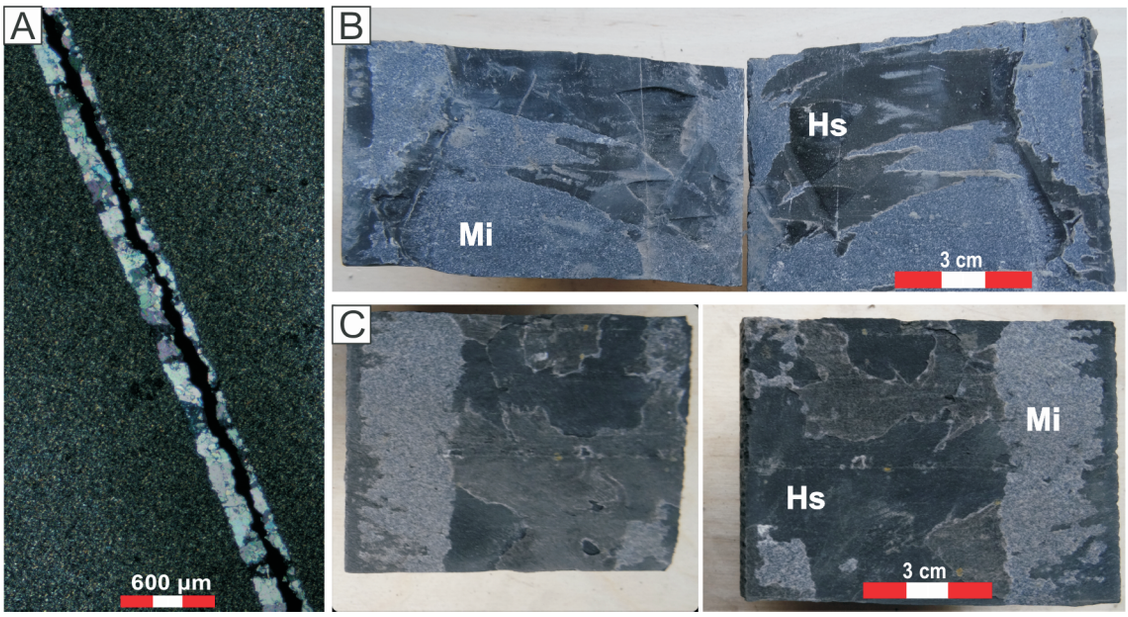

Fig. 4. Typical veins developed on joints

A – a thin-section of a blocky calcite vein cracked within the mineral seal, leaving calcite on both fracture walls; **B** – two counterparts of a joint partially filled with calcite, split within the mineral seal (Mi), leaving calcite on both sides of the crack, creating a symmetrical view; **C** – two counterparts of an entirely filled vein split along the interface between mineral infill (Mi) and host shale (Hs), creating a negative view, and partially within the mineral seal, creating a symmetrical view

veins are mostly intact. Here, on average only 13% of veins are cracked, with a minimum of 8% in the B-4 borehole and a maximum of 30% in the B-7 borehole. Therefore, significant cohesion could be attributed to these veins. The more cohesive vein behaviour of the Prabuty Fm. may be explained by the higher carbonate content of the matrix resulting in effective bonding with the calcite infill of veins. Considering that this cohesive unit separates two gas-productive shale units, this information can be important for designing the optimal placement of the horizontal interval of exploitation boreholes. Strong veins, in spite of their preferential orientation for hydraulic stimulation, might block fracture stimulation, cutting off potentially productive formations from each other (Nelson, 2001).

DIRECTLY ORIENTED CORE AND FRACTURE ORIENTATION ERROR

In the B-1 and B-2 boreholes, the core was directly orientated to the magnetic north by the Multishot Survey Tool (EMF). The core orientation is based on scratching of three nominally continuing scribes on the core surface during its placement into the core barrel. The azimuth of the primary scribe is measured at 25 cm depth intervals. The primary scribe can be recognized by its distance to secondary scribes, which is larger than the distance between secondary ones (Fig. 5). In the core storage facility, the orientation of fractures is measured in relation to the primary scribe, and then the relative orientation is recalculated to the actual one by adding the primary scribe azimuth taken from documentation (Nelson et al., 1987; Lorenz and Cooper, 2017).

Commonly, due to either technological or natural reasons, not all three scribes are carved on the core. Some scribes are usually only partially preserved in poorly consolidated rock (like tuffite) or are not grooved in excessively hard rock (like radiolarite), which are both present in the shale successions analysed. Unfortunately, in the most heavily fractured intervals, the core often becomes so disintegrated that the scribes are not clearly carved. In consequence, an insufficient fracture orientation is obtained from intervals where their orientation would be most desirable.

There are a few sources of possible error in the direct fracture orientation (Nelson et al., 1987; Bobek and Jarosiński, 2018). One of them is the simple inaccuracy of determination of an angular distance between the primary scribe and the strike of the fracture. This systematic error, estimated at 5°, is assumed

Table 2

The statistics of cracked veins in the boreholes analysed, the B-1 borehole is not included due to scarce veins

Borehole	Number of veins	Number of veins split within the mineral seal	Number of veins split along vein/rock interface	% of cracked vein surface
B-2	362	162	21	70.7
B-4	152	12	20	61.6
B-5	106	20	10	36.4
B-6	191	50	19	50.9
B-7	91	12	3	86.8

to be equal for each fracture orientation and therefore is not considered in the further error calculation. Fracture orientation inaccuracy might also stem from rapid rotation of the tool, which results in large jumps of the primary scribe azimuth between measuring points 25 cm apart, combined with an uncertain depth correlation between these points and the core in the box. When the rotation of the tool becomes faster (Fig. 6), the error grows. The same holds for a growing uncertainty in the core depth correlation with the nominal tool depth. This correlation becomes less accurate when the amount of lost core increases. We propose to approximate the angular error (*AE*) in the determination of fracture strike based on the rate of angular rotation of the tool per metre (*RR*) and the precision of the core depth (*CD*) estimation [2]:

$$AE = RR \ \ CD \qquad [2]$$

To simplify the analyses, we assumed a constant *CD* ±10 cm. However, in a more detailed analysis, one may estimate this value for each fracture individually, based on e.g. the percentage of the retrieved core in the box. For instance, for the given constant *CD* and *RR* = 360°/m, occurring in the boreholes analysed, the *AE* = 36°. To avoid contamination of our dataset by poor quality records we have not accepted orientation for which *AE* >20° and considered such fractures as non-oriented. Such an approach is the trade-off between the precision of analysis and the need for having the maximum number of oriented fractures. For the two boreholes, we have counted that >50% of fractures observed in the core have not been oriented successfully. In practice, the use of direct core orientation technology in shale allowed for orientation of a minority of fractures, although the shale is not intensely tectonized. For directly oriented fractures, the *AE* error has been taken into account in the rose diagram construction by applying a blurring procedure as described in chapter *Joint orientation errors on rose diagrams*

JOINTS IN MICRORESISTIVITY SCANNER IMAGES

Interpretation of high-angle strata-bound joints in a scanner image differs in some aspects from the interpretation of other fractures (Williams and Johnson, 2004; Spina et al., 2015; Lai et al., 2018). When the joints are of moderate size and subparallel to the borehole axes, they do not often create a full sinusoidal shape of intersection trace with the borehole wall. Instead, the joint intersection is frequently represented by a fragment of the sinusoid or by two lines, typically tens of centimetres long with a variable angular separation. Correlation of these traces to each other is sometimes uncertain, especially when more than one joint is present in the same stratal interval. The problem of recognizing joints is increased when only part of the borehole wall surface is covered by the scanner image (Fig. 7). In the study boreholes, wall coverage by scanner images reaches 64%, implying that for minor steep joints there is significant probability that the counterpart intersection line is not recorded.

In addition, industrial codes are not tailored to analyse strata-bound joints. They typically do not provide the option of a partial sinusoid matching to trace the joint, that makes it difficult to measure true fracture height and depth. The fracture height, the angular span of fracture intersection (see next paragraph), or type of fracture termination are often not provided in the standard tools. In our study, structural analysis of scanner images was performed using *TechLog* software, which includes the function of partial sinusoid fitting to the fracture; however, we had to measure manually the heights of strata-bound joints.

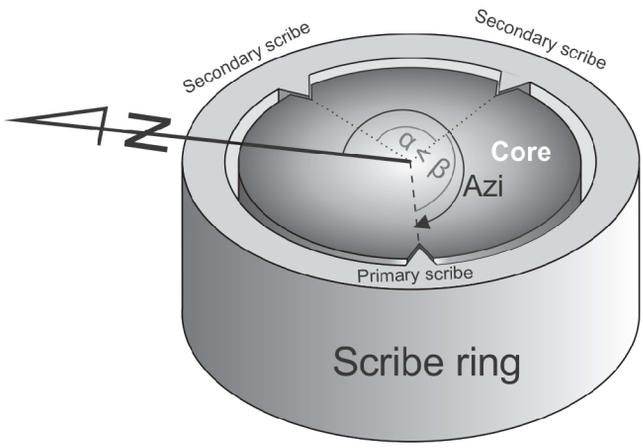

Fig. 5. The method of core orientation used in the MultiShot Survey; based on three scribes on the borehole core surface

The primary scribe is oriented to the magnetic north (Azi). The identification of the primary and secondary scribes is based on the relative angular distance between the scribes: the angle between secondary scribes is smaller than the angle between primary and secondary scribes

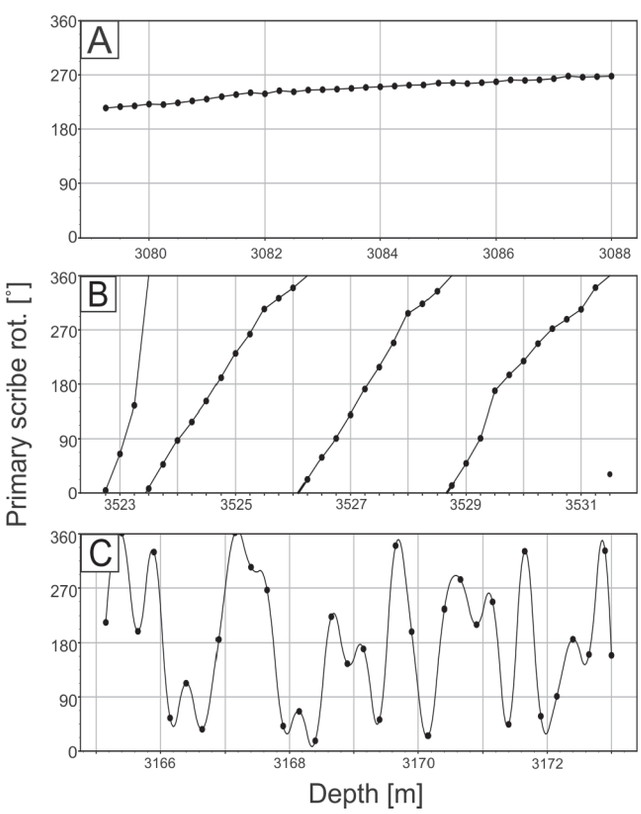

Fig. 6. Examples of study borehole sections showing primary scribe orientation in the function of depth

A – best quality measurements with a relatively stable position of the primary scribe due to the low rotation rate of the tool ~5°/m; **B** – worst quality measurements with a significant orientation error due to a fast rotation rate <180°/m; **C** – fast rotation or vibration of the tool makes the measurements useless for core orientation

Considering the above features of joints, we have distinguished five types of joint record in the scanner images (Fig. 7):

A. The joint intersection represents a full sinusoidal trace, indicating that both ends (in vertical orientation) escape the observation space. In this case, the true height of the joint is unknown, but its orientation is precise.
B. The joint intersection is represented by part of the sinusoid due to one end bounded by strata and the second coming out of the observation space. The true joint height is unknown, the strike is certain, but the accuracy of the dip angle depends on the height of the partial sinusoidal trace.
C. The trace of joint intersection is represented by two separate lines of similar depth range, which fit the intersection sinusoid with high certainty. These traces are specific for strata-bound joints, whose true height is known, and where the orientation is certain.
D. The joint intersection is represented by two or more short lines with an ambiguous coupling to each other or with uncertain sinusoid fitting. This results in a poorly constrained orientation and height of the joint.
E. The joint intersection is represented by a single line trace. If the trace is short, which is common for joints, fitting the sinusoid is highly uncertain or impossible. A satisfactory estimate of joint orientation is impossible and, sometimes, even the presence of a joint is uncertain.

Discrimination of the above types of joint records in a scanner image allows for further data processing, including the credibility of observation or differentiation between the true and partial height of joints, and using them as parameters of analysis. We prefer to use these types of joint records to separate joints of true height in order to compare them with bed thickness or other parameters. The C, D, and E types represent degrees of credibility of fracture record that can be used in statistical analysis e.g. by means of a "blurring procedure" (see further paragraph).

COMPARISON OF JOINT OCCURRENCES IN BOREHOLE CORES AND SCANNER IMAGES

In our previous study (Bobek and Jarosiński, 2018), we have found significant discrepancies between results of core and image log interpretations for the same boreholes and depth intervals. The differences are not only due to drilling-induced fractures. The systematically higher fracture intensity in the scanner image over the core profile was explained by a large number of tiny non-cracked veins that are better recorded by a scanner then by the unaided eye, especially in bright, carbonate-rich formations. By contrast, fracture intensity in intervals enriched in TOC was always higher in the core than in the scanner image, that we related to the hiding of fractures by gas saturation that enhances resistivity, creating an effect of overexposure in scanner images. Apart from these differences, we have also observed that joints are missing in the borehole core due to the simple geometrical reason that the diameter of the borehole is larger than the core diameter. This matters especially with strata-bound joints, which sometimes intersect the borehole wall and do not enter the core space (Fig. 8A).

Imperfect identification of the same fractures in core and scanner records causes difficulties with depth correlation between both sets of data. The difficulties increase with the growing intensity of jointing. To find the joints restricted to the scanner image, we have defined the angular span of the joint intersection in the scanner image. If the angular span is below the value of a certain critical opening angle ( ) the joint should not penetrate the borehole core. The angle depends on the ratio between the borehole (R) and core (r) radius:

$$2\arccos\frac{r}{R} \qquad [3]$$

If the measured angular span of the joint is higher than , at least part of the joint is present also in the core.

Figure 8B shows fracture data filtering from the B-2 borehole interval resulting in a correct correlation between joints in the core and the scanner image. In the given example, the depth of joints in the core is systematically shifted to shallower depths by comparison with the same joints in the scanner image. This kind of filtering allowed us to state that the depth correlation between the log and the core was not exact and an additional offset of up to 1 m is necessary. However, when attempting this kind of correction, one should verify whether the height of joints in the core is true or not. If the height is true, the joint depth in the scanner should be identical with the one measured in the core. But if one end of a joint stretches beyond the core, the mean depths of the joint in the scanner image and the core are not the same due to the difference in the length of their intersection. In the case presented by us (Fig. 8B), the joint height is true and the discrepancy between the core and log depth needs correction.

STATISTICAL ANALYSIS OF JOINTS

WEIGHTED DIAGRAMS OF JOINT ORIENTATION

The conventional way to present fracture orientation is by plotting poles to fracture planes on hemispherical projections (e.g., Seeburger and Zoback, 1982; Fisher et al., 1993; Martel, 1999). Since our study is focused on high-angle joints, we have used simple rose diagrams, which are also frequently applied to reservoir characterization (e.g., Petrie et al., 2012). In standard rose diagrams, each fracture is treated as one record, in spite of its size, accuracy of measurement, or aperture. Hence, e.g. a 10 cm high fracture statistically equals that of one 2 m high. Considering that fracture properties important for a shale reservoir, such as conductivity or susceptibility to stimulation, are dependent on the fracture size (Gutmanis et al., 2018), such a simple conventional approach seems inadequate for joints differing in size by two orders of magnitude. Thus, having determined the true height for the majority of joints, we have used this parameter to weight the rose diagrams of joint strikes.

In our weighted diagrams, we have calculated the cumulative height of joints for every azimuthal class, irrespective of whether the height is true or not. We applied a 10 or 18° angular width for the azimuthal classes, depending on the number of joints in a borehole and their distribution. In this approach, the length of bins in diagrams is given in metres instead of reflecting the numbers of fractures, as in conventional plots (Fig. 9 and Table 3). Another way of scaling the bins is by dividing their summarized height by the length of the borehole profile analysed. Such normalized diagrams provide a better approximation of joint intensity for each azimuthal class, which can be directly represented on such diagrams.

A comparison of conventional and weighted rose diagrams for the boreholes studied shows that the orientation of joint sets in all the boreholes is generally similar for both kinds of diagram. Nevertheless, it reveals some differences in frequency proportions between particular joint sets. For instance, in the B-5 bore-

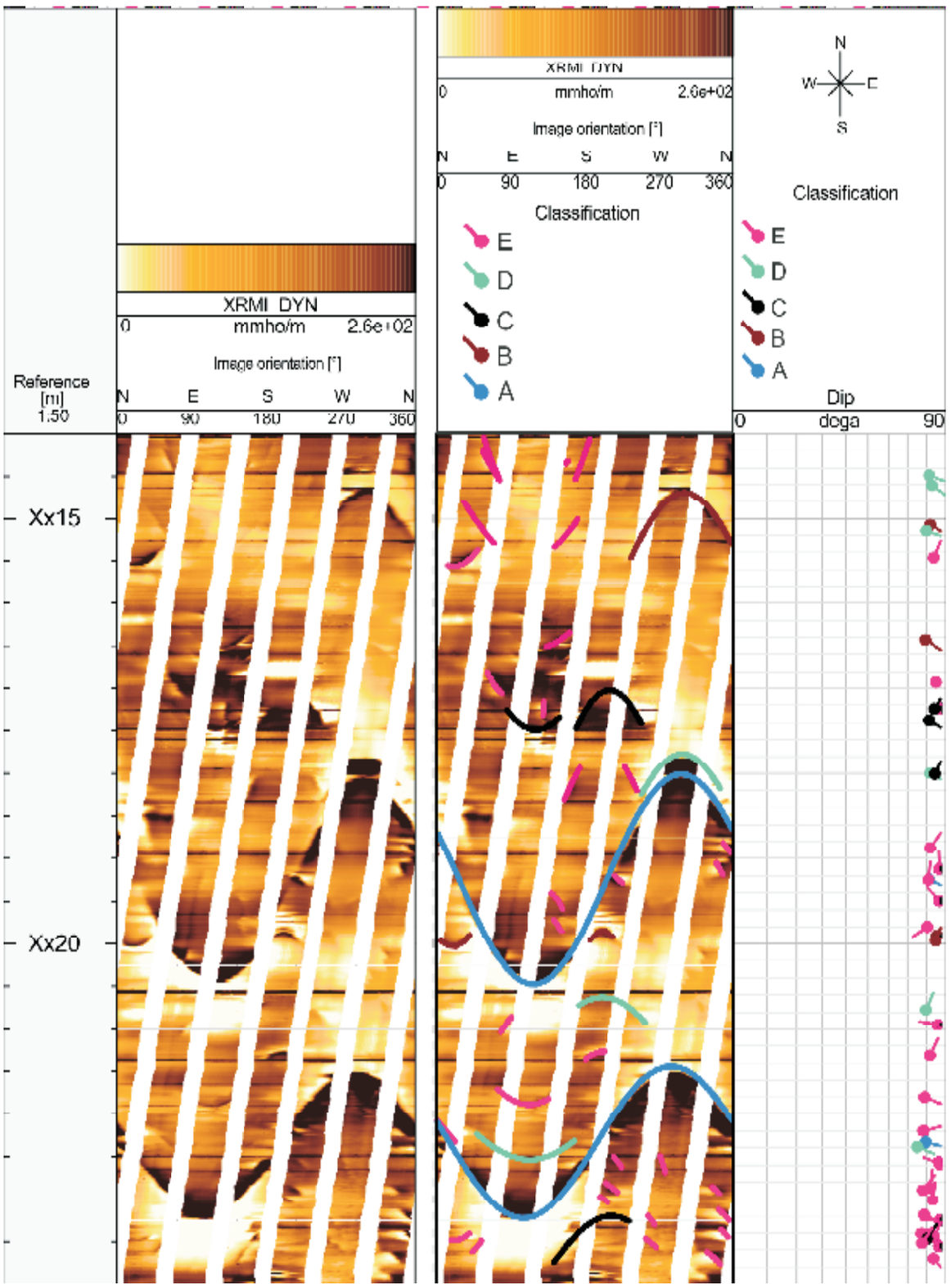

Fig. 7. Example of joints from an XRMI image of the B-2 borehole wall

The left track is before interpretation; the colours of marks correspond to the joint record type (see the legend and the text); note that most of the fractures terminate, at least from one side, at the strata surfaces

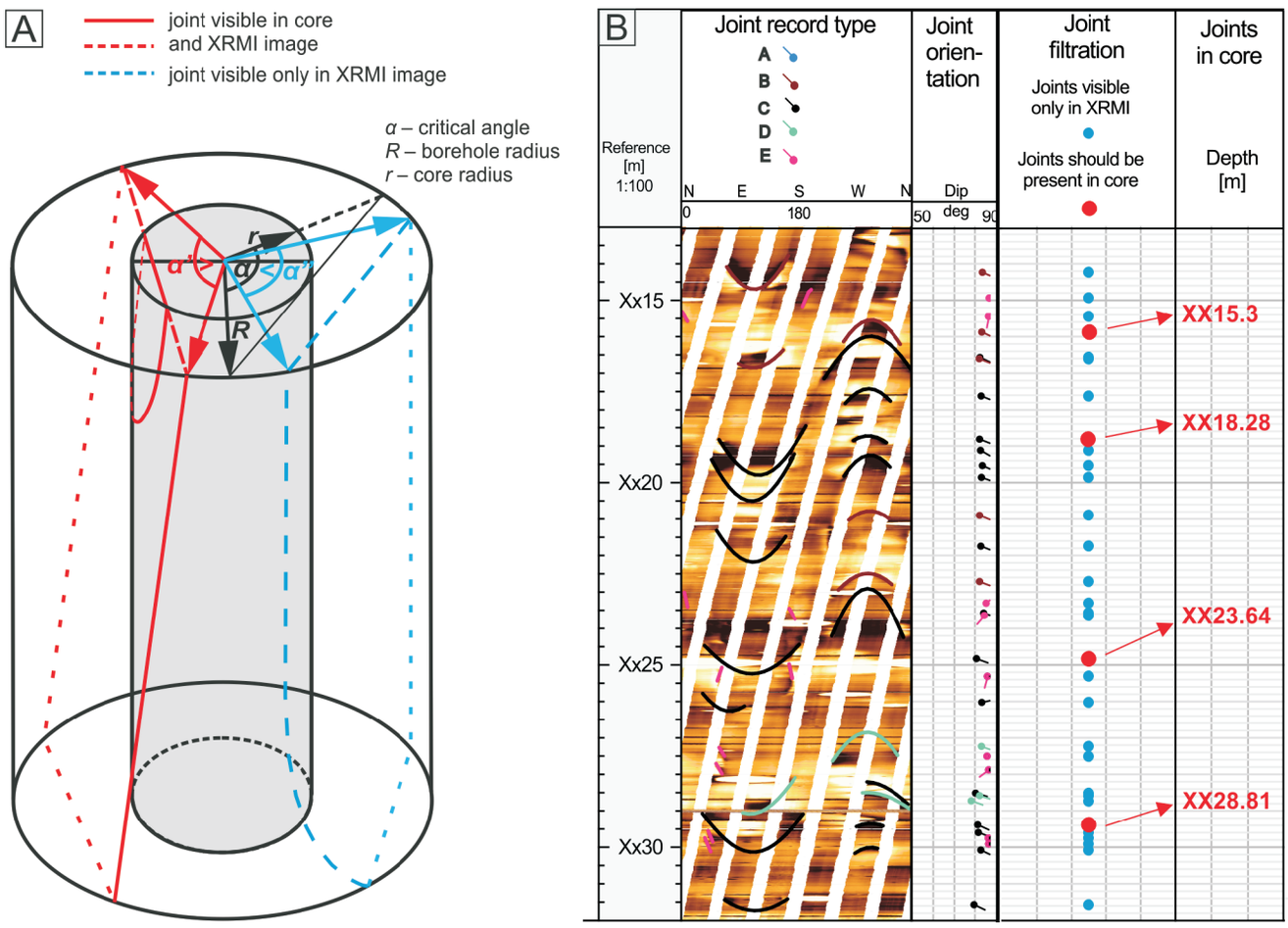

Fig. 8. The principle, and an example of, filtering using the critical opening angle parameter

A – we assumed that the strata-bound joints terminate at the upper surface of the cylinder; at this surface, the critical angle ( ) is stretched on the chord of the borehole circle (radius *R*) and tangential to the core circle (radius *r*); the joint with the angular span ' > is partially represented in the core (red lines), while the joint with the angular span " < is visible only in the scanner image (blue dashed line); **B** – implementation of filtering using a critical angle to the joint data in the B-2 borehole: 1st trace – XRMI scanner image; intersection lines of joints with the record type distinguished are interpreted; 2nd trace – orientation of joints with the type of their record distinguished (marked by colours); 3rd trace – results of filtering pointing to joints present only in the scanner image (blue dots) and joints present also in the borehole core (red dots); 4th trace – the depth of joints observed in the borehole core; note the systematic shift in joint depth between analogue joints in the scanner image and the core (marked with arrows)

hole (Fig. 10) the conventional diagram suggests that there are three joint sets J1, J2, and J3, of comparable intensities. On the weighted diagram, set J1 is unequivocally dominant, while the J2 and J3 sets are subordinate. Such a result is better suited for the regional joint system characterization and allows a better judgment of the significance of certain joint sets that may, for example, control the privileged conductivity direction in a reservoir.

It is also possible to create a diagram weighted by compound parameters, e.g. joint height multiplied by vein aperture (Fig. 11). In such an approach, the length of the bin stands for the integrated area of the veins' cross-section in the azimuthal class of the bin, given in areal units. When normalizing this value by the length of the borehole section analysed, we represent the measure of extension at a given azimuthal class or of the joint set, if the azimuthal class embraces the entire set.

JOINT ORIENTATION ERRORS ON ROSE DIAGRAMS

We have used the angular error of joint orientations, based on directly oriented core (chapter *Directly oriented core and fracture orientation error*), in the construction of the rose diagram. For this purpose, a simple procedure was devised that leads to blurring the less credible records on the diagram among the neighbouring azimuthal classes. To obtain this effect, we start with finding the exact position of a joint strike in the azimuthal class and check if the error bar, given by angular error (*AE* from Eq. 2), extends beyond this class from one or from both sides (Fig. 12). If the azimuthal class range is small in comparison to the error bar, the bin can be distributed to more than two classes. Subsequently, we calculate the percentage of the error bar, which is located in the adjacent class or classes. Finally, the relevant portion of the bin given by the percentage of the error bar, is allocated to the adjacent class or classes, which results in blurring of an individual record with respect to the size of the error bar. If the error bar contains one azimuthal class, the blurring procedure is not applied. In the conventional diagram, the value of the record equals 1 for one joint, so after applying the blurring procedure, fractional numbers of joints in the azimuth classes appear. For the diagrams weighted by the joint height, the blurring effect is proportional to the height of the joint. In this approach we have used a simple proportional distribution of bin in adjacent classes, however, any other distribution is also possible.

Table 3

An example of input data for standard and weighted rose diagram construction for the J1 and J2 joint sets from the B-6 borehole

Angular range [°]	Standard rose diagram	Weighted rose diagram
	J1 set	J1 set
	Number of joints [-]	Total of joint heights [m]
170–180	5	1.07
0–10	7	8.08
10–20	13	7.4
20–30	3	2.39
Total	32	19.36
J2 set	J2 set	
Angular range [°]	Number of joints [–]	Sum of joint heights [m]
100–110	17	7.03
110–120	27	12.67
120–130	9	2.52
130–140	10	1.25
Total	63	23.47

An effect of the blurring procedure is shown, based on directly oriented core data from the B-2 borehole, in which the error bars were determined for 129 successfully oriented joints (AE <20°). The comparison between the three diagrams: a standard one, weighted by joint height and weighted including the blurring (Fig. 13) category, shows that this procedure does not influence the balance between the main fracture sets, but visibly increases the background noise. An additional effect is the appearance of the secondary strike mode within the primary joint set.

DETERMINATION OF JOINT AREA

As the height of joints was measured, we have used this parameter to express the joint intensity as a cumulative area per core/borehole space volume (P_{32}). A straightforward method for determination of the area of fractures with an elliptical shape of intersection with the borehole was given by Narr (1996). Here, we check if a similar approach can be applied for strata-bound joints, with a more complex shape of intersection with a borehole. In a general case, the shape of such an intersection is a portion of ellipse cut off from one or both sides by straight intersection lines with the bedding plane. In the case of a steep joint, the shape of intersection area becomes more rectangular. Finally, considering a vertical joint, we arrive at a rectangular shape of the intersection with a vertical borehole wall. The area of this rectangle is a product of its height, which is measured, and the horizontal dimension, which we call the length of intersection. This length can vary from infinitesimally small to borehole diameter, depending on mutual joint and borehole position. Considering that shifting the borehole position by several centimetres may significantly change the length of a joint intersection, in our approach we have assumed that this length is, to some extent, random. Therefore, the length of the intersection can be expressed by the expected value of the chord length of the circular borehole cross-section (Fig. 9). To find this value, we search for the expected length $E[x]$ (Eq. 4) for one set of parallel chords:

$$E\ x \qquad xf\ x\ dx \tag{4}$$

Solving this equation for the expected joint intersection length ($E[l]$) (Fig. 14A), where d is the borehole diameter, and $f(x)$ is the area of transverse borehole section, gives:

$$E\ l \quad {}_0^{d}\frac{1}{d} f\ x\ dx \quad \frac{1}{d} \quad \frac{d}{2}^{2} \tag{5}$$

Hence, the expected chord length (l) is:

$$l \quad \frac{d}{4} \tag{6}$$

The value calculated should hold for each parallel set of chords, and therefore can be taken for a circle in general.

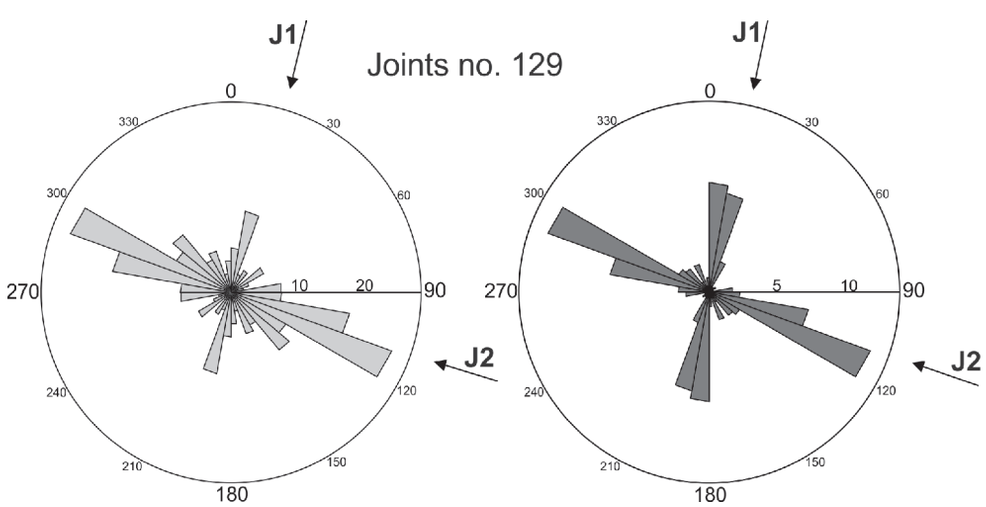

Fig. 9. Comparison between the strike of joints, determined for the same scanner image data from the B-6 borehole

Standard diagram based on the number of joints (left) and a diagram weighted with the height of joints in metres (right); the regional primary J1 and secondary J2 joint sets are marked

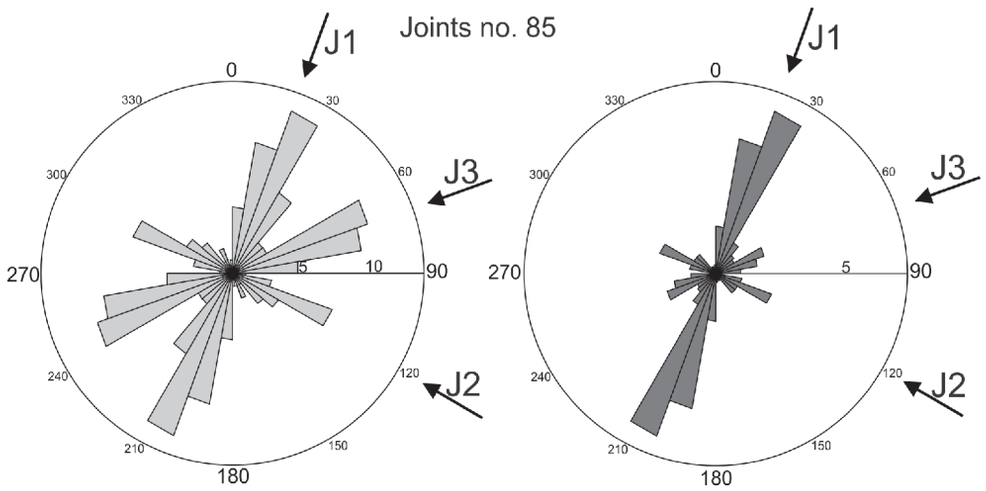

Fig. 10. Diagram of joint strike for the same dataset from the B-5 borehole

Conventional diagram based on the number of joints (left) and a diagram weighted by joint height in metres (right); the most striking difference is seen in the expression of the J3 joint set

The above approach was applied to a special case of a vertical joint in a vertical borehole. But the random character of fracture intersection dependence on borehole position holds for any inclined joint, where at least one end terminates within the borehole space. Therefore, we calculate the area of any strata-bound joint (A_j) using the height (h), the dipping angle ( ) and the constant value of expected length (l) substituted from Equation 6 (Fig. 14B):

$$A_j \quad \frac{hl}{\sin} \quad \frac{dh}{4\sin} \qquad [7]$$

The above solution proposed for strata-bound fractures can be compared with a general solution for inclined fractures with an elliptical intersection with a borehole (Fig. 14B). The fracture area (A_f) might be calculated from two axes of elliptical intersection created by the borehole diameter (d) and the joint height divided by the sine of the dip angle ($a = h/\sin$):

$$A_f \quad \frac{d}{2} \frac{a}{2} \quad \frac{da}{4} \quad \frac{dh}{4\sin} \qquad [8]$$

The result obtained for any fracture escaping the borehole space (Eq. 8) is the same as for any joint in which at least one end terminates on the bedding plane (Eq. 7). Therefore, in spite of the type of fracture intersection with the borehole, we use this simple formula linking the fracture area with its measured height and dip angle.

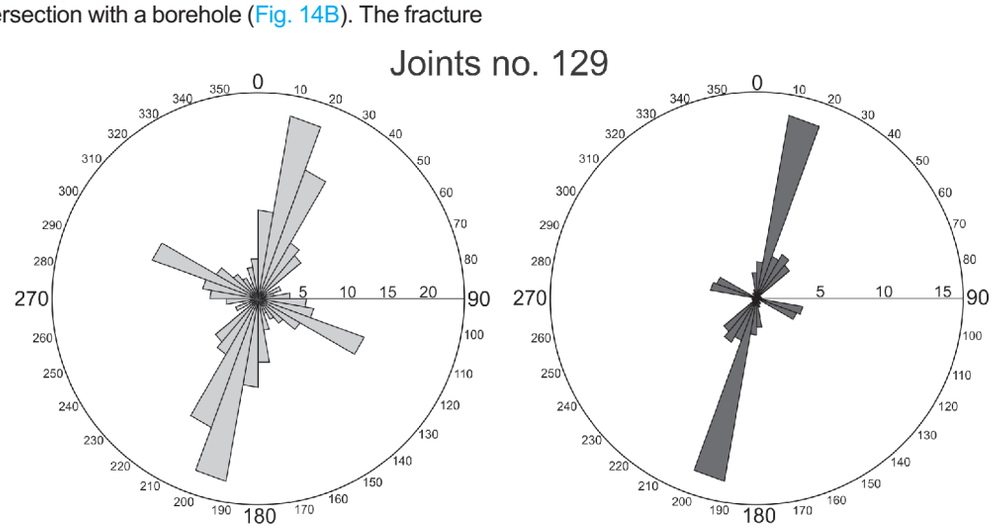

Fig. 11. Diagrams of joint orientation based on the same dataset from the directly oriented core of the B-2 borehole

Conventional diagram, based on the number of joints (left) and a diagram weighted by joint height multiplied by kinematic apertures of joints, expressed in cm^2 (right); this weighting procedure emphasizes the mineralization of the J1 joint set

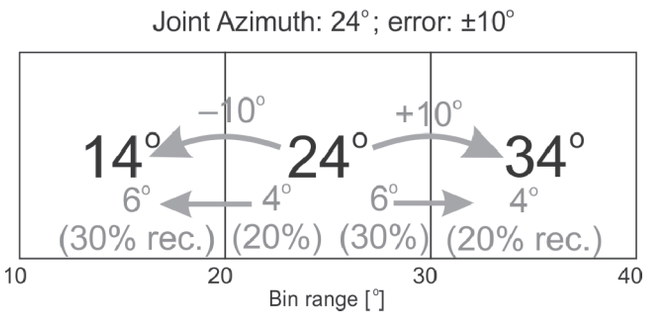

Fig. 12. Scheme showing allocation of part of the joint record to the adjacent bins according to the angular error of joint orientation, used in the blurring algorith

See text for explanation

JOINT INTENSITY PROFILING

In industrial practice, the most common approach is to calculate the fracture profile by means of the moving average method, by counting a number of fractures in a sampling window on each sampling step. In our approach, we have calculated real joint intensity profiles, which are defined by the integrated area of joints in the volume of the core/borehole interval, which is denoted in the literature by P_{32} (Dershowitz and Herda, 1992). The area of each joint surface was calculated according to Equation 8. When using the moving average method, the size of the sampling window and its step should be adjusted to the number of joints and the desired resolution of the fracture profile. In order to collect the representative number of joints in a small borehole space, the window should be long. But the increasing window size decreases the resolution of the fracture intensity profile, blurring its stratification. The trade-off between these opposite tendencies and the representativeness of fracture profiles constructed using scarce borehole data (Barthélémy et al., 2009; Gross et al., 2009; Prioul and Jocker, 2009) is beyond the scope of this study.

In our boreholes, the vast majority of joints show heights in a range of 10–50 cm. When comparing this to the most common 3 m long sampling window and the common 1 m step, it becomes obvious that counting a number of joints in the window is not an appropriate way to address the joint size differentiation. Although the average joints are much smaller than the sampling window, some joints exceed the actual range of the window. In such a case, only part of the joint placed in the window is considered for intensity calculation (Fig. 14C). Therefore, the summarized joint area within the sampling window divided by the core/borehole volume gives the joint intensity (*JI*):

$$JI = \frac{\sum_{i=1}^{n} \frac{h_i \, l}{\sin \alpha_i}}{W_l r^2} \quad [9]$$

where: h_i – the height of i^{th} fracture, l – the expected value of fracture length, α_i – the dip angle, r – the core/borehole radius, W_l – the vertical length of the sampling window.

The calculated intensity value expressed in either m^2/m^3 or m^{-1} is assigned to a bin placed at the depth of the sampling window centre (Fig. 14C).

JOINT INTENSITY STRATIFICATION: A DISCUSSION

In the most common industrial approach, a joint intensity profile is calculated for all fractures regardless of their orientation. Such a solution, less meaningful for reservoir characterization, is justified by the lack of core data orientation, or by scarce fractures giving insufficient representation of fracture sets for their separate statistical analysis. In our analysis, the intensity of jointing was calculated separately for each joint set recognized, the angular range of which has to be predefined based on a previously constructed diagram of joint orientation.

Below, we provide two examples of joint intensity profiles (Fig. 15) in order to show the workflow and performance of the modified methods. The two boreholes were chosen to illustrate extreme cases among the study boreholes: the maximum (B-2) and minimum (B-1) intensity of jointing. In both cases, our analyses integrate borehole core and microresistivity scanner data.

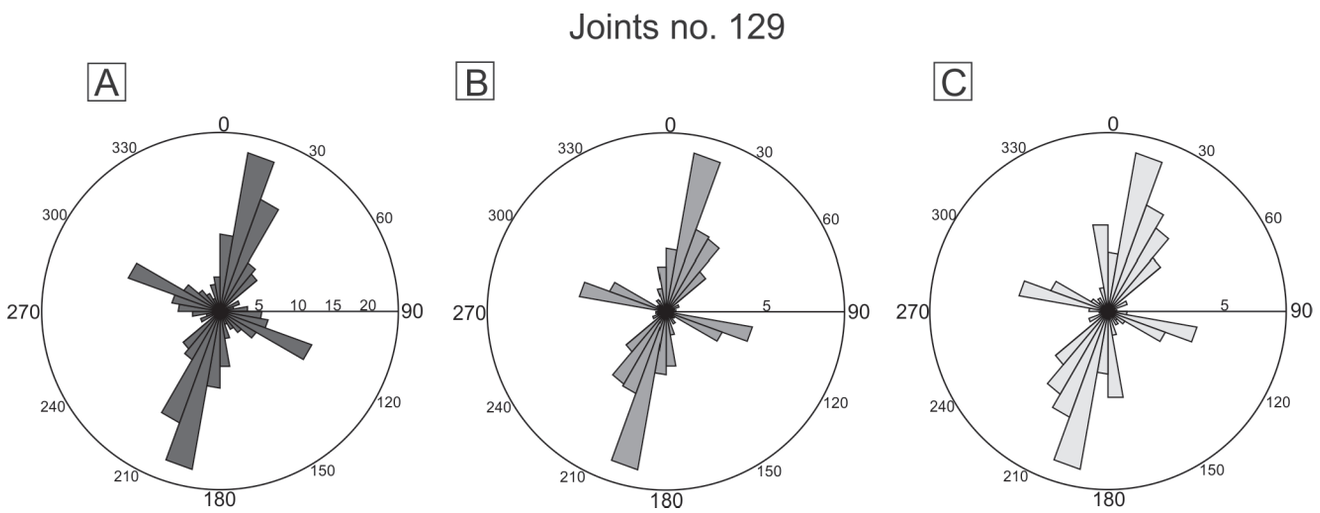

Fig. 13. Joint orientation diagrams constructed for the same interval of the oriented core of the B-2 borehole

A – conventional diagram based on the number of joints; **B** – diagram weighted by joint height in metres; **C** – similar to B but with blurring procedure applied, including the error of joint orientation

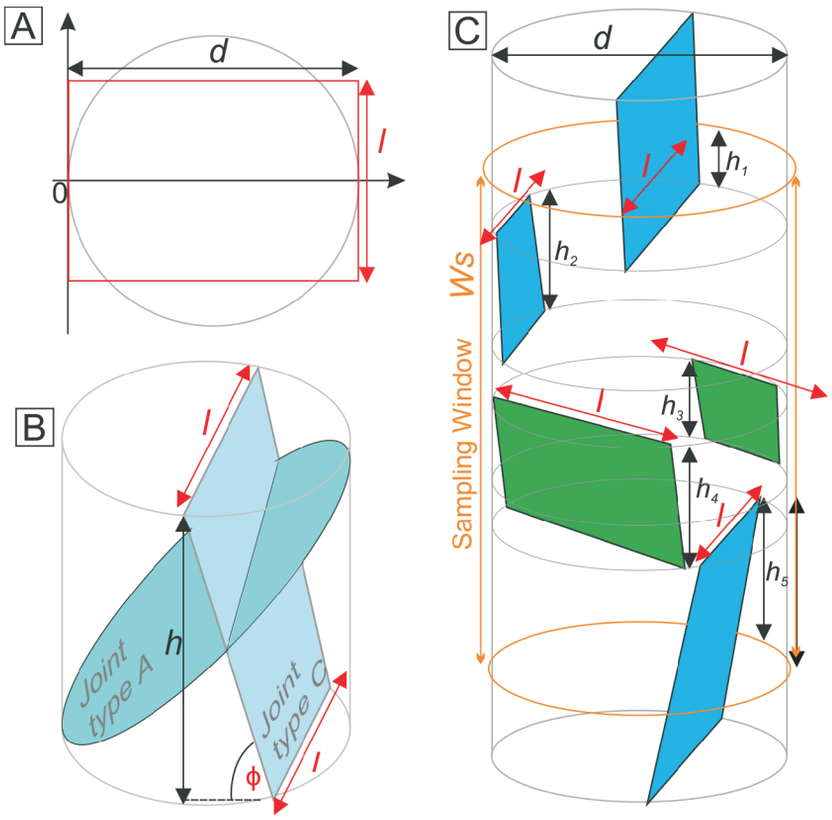

Fig. 14. Schemes for joint intensity calculation

A – the transverse cross-section of a borehole (grey circle) with the expected joint length (*l* – red line) marked, the rectangle (red) created by the borehole diameter (*d*) and the expected value of joint length (*l*) has an area equal to the borehole cross-section area; **B** – two types of joint intersection with the borehole: type A (going beyond the borehole space) creates a sinusoidal intersection on the scanner image, type C (strata-bound on both sides) creating a intersection in the form of two lines, the joint height is always measured in the vertical (borehole axis) direction, the joint area is calculated including the dip angle ; **C** – the scheme shows two joint sets within the sampling window, only that part of a joint's height that falls within the sampling window is included in joint intensity calculation, in spite of the actual joint intersection with the borehole a constant value of the expected length *l* is applied to all joints

The joints depicted in the scanner image were processed with comparative joint filtering in order to find those joints which should be present but are not recognized in the scanner image. Twenty-seven such joints were identified in the B-2 and twenty-one in the B1 borehole; however, most of them were not successfully oriented by the direct orientation tool. Therefore, they do not contribute significantly to the joint set orientation diagram, but indicate the general intensity of the joint system. Based on consistent joint set performance (Figs. 9–11), we have defined the angular ranges of joint strikes for two sets: 0–40° for J1 and 90–130° for J2. Joint intensity profiles were calculated for a constant 3 m-long sampling window and a 1 m sampling step.

In the B-2 borehole, including a large number of joints (735), we were able to obtain good coverage of the borehole profile for the separate joint sets (Fig. 15). The intensity of the most numerous J1 set frequently attains 4 m^{-1} that gives a mean horizontal distance between joints in the range of 25 cm. The intensity of J2 rarely exceeds 2 m^{-1} that gives more than a 50 cm distance between joints. Although these mean distances are comparable to the thickness of the beds, we do not see a direct relation between these quantities as joint intensity changes from bed to bed at a finer wavelength than the size of the sampling window. Despite this, we have observed an interesting pattern of joint intensity distribution for both sets. These profiles exhibit a clustering of joint intensity, which is comparable to the range of the lithologically and mechanically consistent units that were predefined for the B-2 borehole, based on a set of geophysical and mechanical parameters (Pachytel et al., 2017) before the results of our joint study were completed. A clear decrease of joint intensity is associated with the vicinity of interfaces between the consistent mechanical units. We do not explore the reasons for these intensity changes, but can conclude that detailed processing of joint data in a borehole may give results precise enough to analyse the structural stratification of a shale succession. We can observe that the application of a 3 m sampling window was enough to obtain a continuous J1 intensity profile. This window is, however, insufficient for the J2 profile, which shows some gaps in joint representation. This is not surprising when one considers the 0.1 m^3 volume of the borehole space within the sampling window.

For comparison, we also provide a joint intensity profile for the B-1 borehole (Fig. 15), in which joints are the least numerous among the six boreholes studied. Here, the intensity of joints reaches 2 m^{-1} only in the Prabuty Fm. and in the bottom interval of the black shale. The most jointed, the marly Prabuty Fm. is also the most brittle due to increased carbonate content (Pachytel et al., 2017). In this formation, we can observe that the intensity of the J2 joint set is higher than the J1 set, which is important information for reconstruction of the evolution of mechanical properties of this unit against the background of stress field changes. The intensity profiles of individual joint sets are not continuous, suggesting unreliable joint data representation. Although some clustering of joint intensity might be visible, we would treat this with caution as regards further interpretation of joint set changes in the borehole profile, due to the scarcity of data.

The difference in jointing between the B-1 and B-2 boreholes is all the more intriguing in that these boreholes are located at a distance of ~20 km from each other. Considering that joints in the Baltic Basin were triggered by a natural hydraulic fracturing mechanism driven by overpressure induced by gas generation, we have hypothesized that less intense jointing in the B-1 borehole might result from the significantly lower TOC content by comparison with the B-2 borehole.

For practitioners, a significant doubt may arise as to the sense of constructing such accurate joint profiles in reservoir characterization. At the present stage of development, it is difficult to imagine including such small joints in the useful discrete fracture network model at shale reservoir scale. However, discrete joints can be included in smaller-scale models of mechanically and structurally homogeneous successions that can be

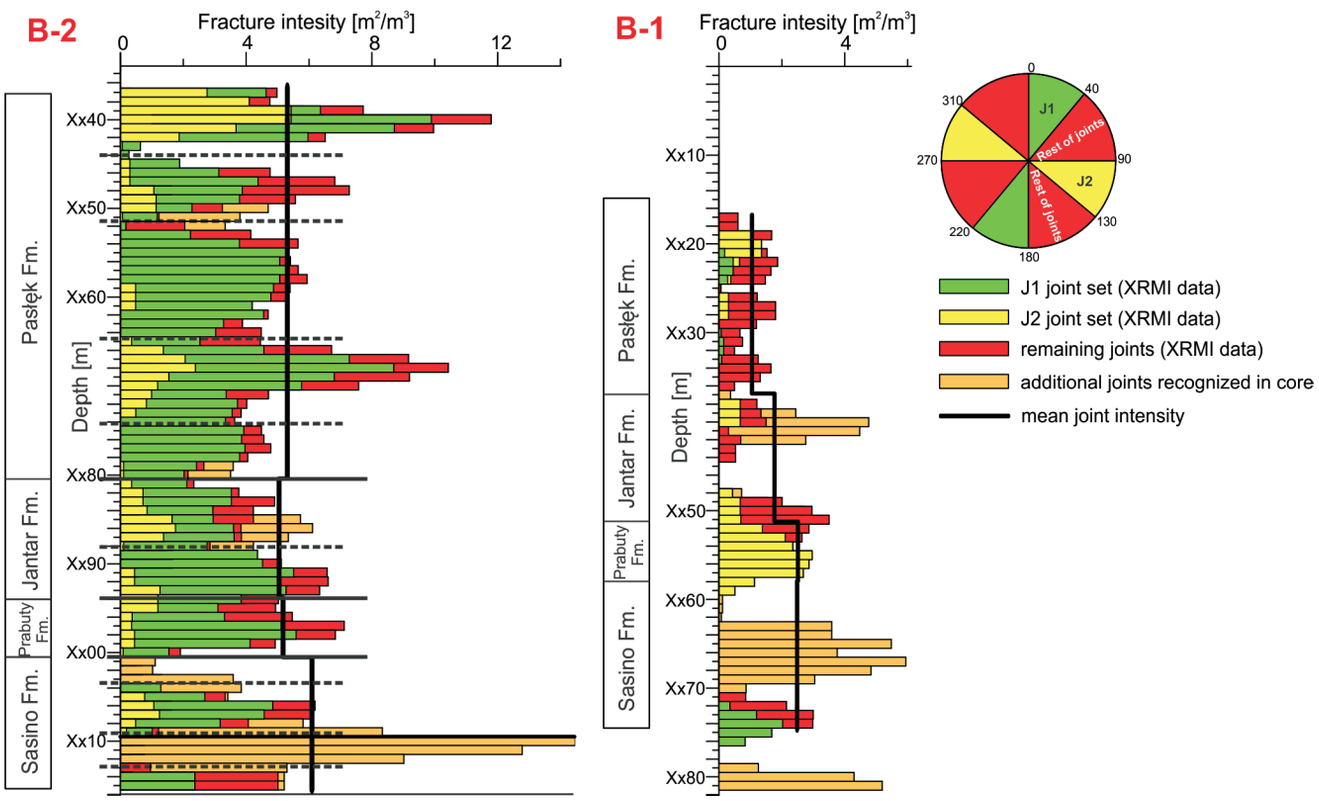

Fig. 15. Joint intensity profiles produced after application of the modified moving average method with a 1 m sampling step and a 3 m window size for the B-2 and B-1 boreholes

The profiles calculated for the J1 (green), J2 (yellow) and the rest of the joints (red) are shown in the form of the stacked bar plot; the mean values for the lithostratigraphic formations are shown by black lines; the division of mechanically consistent units in the B-2 profile (dashed black lines) reveals similarities with the clustering in the joint intensity pattern; the rose diagram shows a range of strike azimuths of the J1 and J2 joint sets

applied to the modeling of stress-sensitive and anisotropic permeability. Increasing the precision of the fracture description, including joints, is perhaps slightly more time-consuming but, in our opinion, worthwhile, especially bearing in mind the cost of obtaining information from deep boreholes.

CONCLUSIONS

Joints, being the most common penetrative fractures in shale successions, are insufficiently addressed in reservoir characterization based on borehole data. Conventionally used methods of fracture analysis of boreholes are adjusted to medium and large fractures that pass through the entire core or borehole wall. They are not adjusted to strata-bound joints in flat-lying shale reservoirs penetrated by vertical boreholes, which is a typical configuration for exploration boreholes in shale reservoirs. In this case, joints reveal their true height, a parameter which is not included in recent analysis methods.

Modifications to fracture analysis, described in this paper, were tested on borehole core and microresistivity scanner data derived from six vertical boreholes penetrating the Lower Paleozoic gas-bearing shale formations of the Baltic Basin. Most fractures are identified as joints of extensional origin. These joints are clustered in two orthogonal sets: a principal J1 set, NNE–SSW oriented, and a subordinate J2 set, WNW–ESE oriented. These joints comprise calcite veins which are secondarily cracked in the relaxed borehole core.

We have systematically observed the percentage of cracked veins and the style of vein splitting in the core. Assuming that core cracking due to relaxation during extraction to the surface is a similar phenomenon to effective stress relaxation during hydraulic treatment, these features can be a semi-quantitative indicator of vein/joint cohesion. We have also proposed quantifying the splitting of calcite veins, considering calcite left on neither, one, or both fracture faces for prediction of sealing barriers for gas drainage to the stimulated conductive joint network. Some stratification of the vein cracking phenomenon was observed, which might be important for reservoir stimulation.

We have distinguished five types of joint intersection with the borehole wall in the scanner record. Adopting such classification allows further processing of joint data in terms of the true height of joints and the quality of their interpretation.

For integrated interpretation of core and scanner data, we have introduced filtering of scanner-derived fractures using the concept of a critical joint opening angle in order to separate joints which, for geometrical reasons, should not be present in the borehole core. In heavily jointed shale, such data filtering makes it easier to find the same joint in core and in the scanner image, improving the core-log depth correlation and facilitating the orientation of the joint in a core within a dense joint system.

Having access to directly oriented core, we have proposed evaluation of errors in joint strike determination based on the rate of tool rotation and the uncertainty of the core depth control. In our data, due to the cumulative effect of several orientation errors, only <50% of joints observed in the core have been

successfully oriented. For joints with evaluated orientation errors, we have proposed a procedure of blurring less accurate records on the orientation rose diagram.

The simple geometry of vertical exploration boreholes, horizontal bedding, and high-angle strata-bound joints, typical of shale reservoirs, allow us to measure the true height of the majority of joints in the boreholes studied, which varies across wide ranges: 2–200 cm, for core data, and 5–430 cm for scanner data.

The joint height was incorporated in the construction of orientation rose diagrams, which provide more precise reservoir characterization than do conventional diagrams based on the number of joints. An analogous weighting procedure can be extended, for example, to incorporate the apertures of mineralized joints.

We have checked that the same formula can be used to evaluate the area of strata-bound joint intersection with the borehole as for any inclined fracture of an elliptical shape of intersection. The concept of the expected value of joint length intersection with the borehole was used to simplify the problem as regards measuring the complex geometry of joints terminating on bedding planes. The joint area parameter was used in the profiling of joint intensity.

The application of these methods in two boreholes revealed marked structural stratification of the shale reservoir. In the borehole with high joint intensity we have shown that the joint intensity correlates with mechanically consistent units of several metres thickness. However, even precise methods of joint analysis of this kind have limitations due to the small volume of borehole space.

Acknowledgements. We are grateful to the Polish Oil and Gas Co., which has provided us with borehole data, and to Schlumberger for providing software used for borehole scanner interpretation. We also thank our colleague M. Dzikowski from the Computational Geology Laboratory for sharing valuable ideas with us, and the reviewers, V. Guerriero and A.T. Solecki, for insightful comments that improved the text of the paper. The research was part of the BG2/SHALEMECH/14 research project funded by the Polish National Centre for Research and Development (NCBR). The paper was prepared with support from the Polish Geological Institute (project No. 62.9012.1923.00.0).

REFERENCES

Barthélémy, J.-F., Guiton, M.L.E., Daniel, J.-M., 2009. Estimates of fracture density and uncertainties from well data. International Journal of Rock Mechanics and Mining Sciences, **46**: 590–603.

Bobek, K., Jarosiński, M., 2018. Parallel structural interpretation of drill cores and microresistivity scanner images from gas-bearing shale (Baltic Basin, Poland). Interpretation, **6**: SH25–SH38.

Bobek, K., Jarosiński, M., Pachytel, R., 2017. Tectonic structures in shale that you do not include in your reservoir model. Presented at the 51st U.S. Rock Mechanics/Geomechanics Symposium, American Rock Mechanics Association, San Francisco, California. https://www.onepetro.org/conference-paper/ARMA-2017-0079

Boro, H., Rosero, E., Bertotti, G., 2014. Fracture-network analysis of the Latemar Platform (northern Italy): integrating outcrop studies to constrain the hydraulic properties of fractures in reservoir models. Petroleum Geoscience, **20**: 79–92.

Brown, J., Davis, B., Gawenkar, K., Kumar, A., Li, B., Miller, C.K., Laronga, R., Schlicht, P., 2015. Imaging: getting the picture downhole. Oilfield Review, **27**: 4–21.

Dershowitz, W., Hermanson, J., Follin, S., Mauldon, M., 2000. Fracture Intensity Measures in 1-D, 2-D, and 3-D at Äspö, Sweden. Presented at the 4th North American Rock Mechanics Symposium, American Rock Mechanics Association, Seattle, Washington. https://www.onepetro.org/conference-paper/ARMA-2000-0849

Dershowitz, W.S., Herda, H.H., 1992. Interpretation of fracture spacing and intensity. Presented at the The 33rd U.S. Symposium on Rock Mechanics (USRMS), American Rock Mechanics Association, Santa Fe, New Mexico. https://www.onepetro.org/conference-paper/ARMA-92-0757

Doblas, M., 1998. Slickenside kinematic indicators. Tectonophysics, **295**: 187–197.

Engelder, T., Lash, G.G., Uzcátegui, R.S., 2009. Joint sets that enhance production from Middle and Upper Devonian gas shales of the Appalachian Basin. AAPG Bulletin, **93**: 857–889.

Feldman-Olszewska, A., Roszkowska-Remin, J., 2016. Lithofacies of the Ordovician and Silurian formations prospective for shale gas/oil in the Baltic and Podlasie-Lublin areas (in Polish with English summary). Przegląd Geologiczny, **64**: 968–975.

Fisher, N.I., Lewis, T., Embleton, B.J.J., 1993. Statistical Analysis of Spherical Data. Cambridge University Press, Cambridge.

Fu, P., Johnson, S.M., Carrigan, C.R., 2013. An explicitly coupled hydro-geomechanical model for simulating hydraulic fracturing in arbitrary discrete fracture networks. International Journal for Numerical and Analytical Methods in Geomechanics, **37**: 2278–2300.

Gale, J.F.W., Laubach, S.E., Olson, J.E., Eichhubl, P., Fall, A., 2014. Natural fractures in shale: a review and new observations. AAPG Bulletin, **98**: 2165–2216.

Gale, J.F.W., Reed, R.M., Holder, J., 2007. Natural fractures in the Barnett Shale and their importance for hydraulic fracture treatments. AAPG Bulletin, **91**: 603–622.

Grasselli, G., Lisjak, A., Mahabadi, O.K., Tatone, B.S.A., 2015. Influence of pre-existing discontinuities and bedding planes on hydraulic fracturing initiation. European Journal of Environmental and Civil Engineering, **19**: 580–597.

Gross, M., Lukas, T.C., Schwans, P., 2009. Application of Mechanical Stratigraphy to the Development of a Fracture-Enhanced Reservoir Model, Polvo Field, Campos Basin, Brazil. Presented at the AAPG Annual Convention, AAPG, Denver, Colorado. http://www.searchanddiscovery.com/pdfz/documents/2009/20080gross/images/gross.pdf.html

Guerriero, V., Dati, F., Giorgioni, M., Iannace, A., Mazzoli, S., Vitale, S., 2015. The role of stratabound fractures for fluid migration pathways and storage in well bedded carbonates. Italian Journal of Geosciences, **134**: 383–395.

Guerriero, V., Mazzoli, S., Iannace, A., Vitale, S., Carravetta, A., Strauss, C., 2013. A permeability model for naturally fractured carbonate reservoirs. Marine and Petroleum Geology, **40**: 115–134.

Gutmanis, J., Oró, L.A., Díez-Canseco, D., Chebbihi, L., Awdal, A., Cook, A., 2018. Fracture analysis of outcrop analogues to support modelling of the subseismic domain in carbonate reservoirs, south-central Pyrenees. Geological Society Special Publications, **459**: 139–156.

Helgeson, D.E., Aydin, A., 1991. Characteristics of joint propagation across layer interfaces in sedimentary rocks. Journal of Structural Geology, **13**: 897–911.

Hooker, J.N., Laubach, S.E., Marrett, R., 2013. Fracture-aperture size-frequency, spatial distribution, and growth processes in strata-bounded and non-strata-bounded fractures, Cambrian

Mesón Group, NW Argentina. Journal of Structural Geology, **54**: 54–71.

Jarosiński, M., 2006. Recent tectonic stress field investigations in Poland: a state of the art. Geological Quarterly, **50** (3): 303–321.

Johri, M., Zoback, M.D., 2013. The Evolution of Stimulated Reservoir Volume during Hydraulic Stimulation of Shale Gas Formations. Presented at the SPE/AAPG/SEG Unconventional Resources Technology Conference, Unconventional Resources Technology Conference, Denver, Colorado. https://doi.org/10.1190/urtec2013-170

Ladeira, F.L., Price, N.J., 1981. Relationship between fracture spacing and bed thickness. Journal of Structural Geology, **3**: 179–183.

Lai, J., Wang, G., Wang, S., Cao, J., Li, M., Pang, X., Han, C., Fan, X., Yang, L., He, Z., Qin, Z., 2018. A review on the applications of image logs in structural analysis and sedimentary characterization. Marine and Petroleum Geology, **95**: 139–166.

Laubach, S.E., Lamarche, J., Gauthier, B.D.M., Dunne, W.M., 2018. Spatial arrangement of faults and opening-mode fractures. Journal of Structural Geology, **108**: 2–15.

Lerche, I., Narr, W., 1986. Estimating Subsurface Fracture Density in Core: Effects Resulting From Variable Fracture Spacing. SPE Formation Evaluation, **1**: 249–258.

Li, B., 2014. Natural Fractures in Unconventional Shale Reservoirs in US and their Roles in Well Completion Design and Improving Hydraulic Fracturing Stimulation Efficiency and Production. Presented at the SPE Annual Technical Conference and Exhibition, Society of Petroleum Engineers, Amsterdam. https://doi.org/10.2118/170934-MS

Li, L., Lee, S.H., 2008. Efficient field-scale simulation of black oil in a naturally fractured reservoir through discrete fracture networks and homogenized media. SPE Reservoir Evaluation & Engineering, **11**: 750–758.

Lorenz, J.C., Cooper, S.P., 2020. Applied Concepts in Fractured Reservoirs. John Wiley & Sons, Chirchester.

Lorenz, J.C., Cooper, S.P., 2017. Atlas of Natural and Induced Fractures in Core. John Wiley & Sons, Oxford.

Mandal, N., Deb, S.K., Khan, D., 1994. Evidence for a non-linear relationship between fracture spacing and layer thickness. Journal of Structural Geology, **16**: 1275–1281.

Martel, S.J., 1999. Analysis of fracture orientation data from boreholes. Environmental & Engineering Geoscience, **5**: 213–233.

Massiot, C., Townend, J., Nicol, A., McNamara, D.D., 2017. Statistical methods of fracture characterization using acoustic borehole televiewer log interpretation. Journal of Geophysical Research: Solid Earth, **122**: 6836–6852.

Narr, W., 1991. Fracture density in the deep subsurface: techniques with application to Point Arguello oil field. AAPG Bulletin, **75**: 1300–1323.

Narr, W., 1996. Estimating Average Fracture Spacing in Subsurface Rock. AAPG Bulletin, **80**: 1565–1585.

Nelson, R., 2001. Geologic Analysis of Naturally Fractured Reservoirs, 2nd ed. Elsevier, USA.

Nelson, R.A., Lenox, L.C., Ward, B.J., 1987. Oriented core: its use, error and uncertainty. AAPG Bulletin, **71**: 357–367.

Odling, N.E., 1997. Scaling and connectivity of joint systems in sandstones from western Norway. Journal of Structural Geology, **19**: 1257–1271.

Odling, N.E., Gillespie, P., Bourgine, B., Castaing, C., Chiles, J.P., Christensen, N.P., Fillion, E., Genter, A., Olsen, C., Thrane, L., Trice, R., Aarseth, E., Walsh, J.J., Watterson, J., 1999. Variations in fracture system geometry and their implications for fluid flow in fractures hydrocarbon reservoirs. Petroleum Geoscience, **5**: 373–384.

Pachytel, R.W., Jarosinski, M., Bobek, K., 2017. Geomechanical Stratification in a Shale Reservoir and Its Correlation With Natural Fractures: Case From Pomeranian Basin (Poland). Presented at the 51st U.S. Rock Mechanics/Geomechanics Symposium, American Rock Mechanics Association, San Francisco, California. https://www.onepetro.org/conference-paper/ARMA-2017-0077

Peacock, D.C.P., 2006. Predicting variability in joint frequencies from boreholes. Journal of Structural Geology, **28**: 353–361.

Petrie, E., Jeppson, T., Evans, J., 2012. Predicting rock strength variability across stratigraphic interfaces in caprock lithologies at depth: correlation between outcrop and subsurface. Environmental Geosciences, **19**: 125–142.

Podhalańska, T., Waksmundzka, M.I., Becker, A., Roszkowska-Remin, J., 2016. Investigation of the prospective areas and stratigraphic horizons of the unconventional hydrocarbon resources in Poland: new results and future research directions (in Polish with English summary). Przegląd Geologiczny, **64**: 953–962.

Poprawa, P., Šliaupa, S., Stephenson, R., Lazauskien, J., 1999. Late Vendian–Early Paleozoic tectonic evolution of the Baltic Basin: regional tectonic implications from subsidence analysis. Tectonophysics, **314**: 219–239.

Prioul, R., Jocker, J., 2009. Fracture characterization at multiple scales using borehole images, sonic logs, and walkaround vertical seismic profile. AAPG Bulletin, **93**: 1503–1516.

Ramsay, J.G., Huber, M.I., 1987. Techniques in Modern Structural Geology. Volume 2: Folds and Fractures. Academic Press, London.

Salehi, I.A., Ciezobka, J., 2013. Controlled Hydraulic Fracturing of Naturally Fractured Shales – a Case Study in the Marcellus Shale Examining How to Identify and Exploit Natural Fractures. Presented at the SPE Unconventional Resources Conference-USA, Society of Petroleum Engineers, Woodlands, Texas. https://doi.org/10.2118/164524-MS

Schmitt, D.R., Currie, C.A., Zhang, L., 2012. Crustal stress determination from boreholes and rock cores: Fundamental principles. Tectonophysics, **580**: 1–26.

Seeburger, D.A., Zoback, M.D., 1982. The distribution of natural fractures and joints at depth in crystalline rock. Journal of Geophysical Research, **87**: 5517–5534.

Spina, V., Borgomano, J., Nely, G., Shchukina, N., Irving, A., Neumann, C., Neillo, V., 2015. Characterization of the Devonian Kharyaga carbonate platform (Russia): integrated and multiscale approach. AAPG Bulletin, **99**: 1771–1799.

Taghichian, A., Zaman, M., Devegowda, D., 2014. Stress shadow size and aperture of hydraulic fractures in unconventional shales. Journal of Petroleum Science and Engineering, **124**: 209–221.

Van Noten, K., Sintubin, M., 2010. Linear to non-linear relationship between vein spacing and layer thickness in centimetre- to decimetre-scale siliciclastic multilayers from the High-Ardenne slate belt (Belgium, Germany). Journal of Structural Geology, **32**: 377–391.

Watkins, H., Bond, C.E., Healy, D., Butler, R.W.H., 2015. Appraisal of fracture sampling methods and a new workflow to characterise heterogeneous fracture networks at outcrop. Journal of Structural Geology, **72**: 67–82.

Williams, J.H., Johnson, C.D., 2004. Acoustic and optical borehole-wall imaging for fractured-rock aquifer studies. Journal of Applied Geophysics, Non-Petroleum Applications of Borehole Geophysics, **55**: 151–159.

Wiprut, D., Zoback, M.D., 2000. Fault reactivation and fluid flow along a previously dormant normal fault in the northern North Sea. Geology, **28**: 595–598.

Wu, H., Pollard, D., 1995. An experimental study of the relationship between joint spacing and layer thickness. Journal of Structural Geology, **17**: 887–905.

Zoback, M.H., Kohli, A., Das, I., McClure, M., 2012a. The Importance of Slow Slip on Faults During Hydraulic Fracturing Stimulation of Shale Gas Reservoirs. Presented at the Society of Petroleum Engineers. https://doi.org/10.2118/155476-MS

Zoback, M., Kohli, A., Das, I., McClure, M., 2012b. The Importance of Slow Slip on Faults During Hydraulic Fracturing Stimulation of Shale Gas Reservoirs. Presented at the Society of Petroleum Engineers, Pittsburgh, Pennsylvania. https://doi.org/10.2118/155476-MS